Ironmaking & Steel making **W. Feng, F. Qin & H. Long (2016)**
DOI: 10.1080/03019233.2016.1264145

Hot workability analysis and processing parameters optimization for 20CrMnTiH steel combing processing map with microstructure

Wei FENG[a,b], Fei QIN[a], Hui LONG[b,*]

[a] School of Materials Science and Engineering, Wuhan University of Technology, Wuhan 430070, China

[b] Department of Mechanical Engineering, The University of Sheffield，Sheffield S1 3JD，UK

Contact emails: fengwei@whut.edu.cn, 1308806259@qq.com, h.long@sheffield.ac.uk

Abstract: The processing map of 20CrMnTiH steel is developed by developing the dynamic material model (DMM) according to the hot compression experiments, performed on a Gleeble-3500 thermal-simulator at the temperature range of 850-1150℃ and the strain rate of 0.01-1s^{-1}. Hot workability characteristics of 20CrMnTiH steel are analyzed based on the developed processing map. The safe deformation regions with a higher energy dissipation efficiency η exhibit the dynamic recrystallization (DRX) mechanism and show fine and homogeneous microstructure. The unstable regions with negative instability coefficient ξ occur at both lower temperature with all strain rates and at high temperature with high strain rate at the strain of 0.2. The area of instability gradually decreases with the increasing strain and only appears at lower temperature and higher strain rate when the strain is above 0.2. The unstable regions indicate the flow localization by microstructure analysis. Combining with the developed processing map with DRX behavior, the optimal values of hot processing parameters for 20CrMnTiH steel are obtained to achieve good hot workability and small grain sizes at the process parameters ranged at 1036-1070℃/0.1-1s^{-1} and 918-985℃/0.01-0.014s^{-1}.

Keywords 20CrMnTiH steel; hot workability; optimization of processing parameters; processing map; DRX behavior

1. Introduction

Hot workability of metals refers to the plastic deformation ability at high temperature without the occurrence of fracture or flow localization [1]. During hot processing, the deformed material is of different microstructures under different temperature and strain conditions. Flow instability may also take place under some conditions of process parameters, which lead to some defects of the finished part. Therefore, it's very important to understand the hot workability of metal materials to evaluate the safe deformation domains and avoid plastic instability or defects in hot processing.

DOI: 10.1080/03019233.2016.1264145

In the last two decades, the processing map, a product of the Dynamic Material Model (DMM) developed by Prasad et al. [2], has been widely used for all kinds of materials to estimate the hot workability, to control the microstructure and to optimize the hot processing parameters in bulk metal forming [3]. Y. V. R. K. Prasad and K. P. Rao studied the hot workability of electrolytic tough pitch copper and rolled AZ31 magnesium alloy plate by using processing maps, respectively [4,5]. R. S. Septimio et al evaluated the hot workability of microalloyed steels 38MnSiVS5 and 0.39C1.47Mn and obtained the instability domains by constructing the processing maps to identify the safe regions for metalworking [6]. H. Rastegari et al used the processing maps to evaluate the material flow behavior and to define different domains and instability regimes showing various microstructural mechanisms as well as to identify the safe processing window without defects during warm forming of the eutectoid steel [7]. Zhinan Yang et al determined the expanded instability region of the low carbon bainitic steel, 29MnSiCrAlNiMo, by constructing the processing maps at different strains and optimized the processing parameters by combining the processing maps with microstructural observation [8]. Yang Cheng et al studied the metadynamic recrystallization(MDRX) behavior and characteristics of HR3C austenitic heat-resistant stainless steel by combining the kinetic equations of MDRX and hot processing maps and obtained the stability domain [9]. Li Miaoquan and Zhang Xiaoyuan optimized the forging parameters of TC11 alloy based on the processing maps [10]. Quan et al. studied the intrinsic workability of as-extruded 42CrMo high-strength steel, the optimal working parameters was identified by processing maps and validated by microstructure observations [11].

20CrMnTiH steel is a low-carbon alloy steel and widely used to manufacture the transmission components, such as gears, ring gears and gear shafts. The previous researches on 20CrMnTiH steel mainly focused on the material constitutive modeling and flow behavior based on the hot compression experiments. It found that average grain size varied with the deformation temperature and strain rate during hot deformation [12-14]. Their results are useful in developing the Finite Element (FE) model to simulate hot forming of gear parts made of 20CrMnTiH steel by applied the constitution equations obtained in [12-14]. However, these results cannot be used to describe the safe region with good hot workability and instability regions that should be avoided during hot forming process.

This paper is aimed to investigate the hot workability characteristic and obtain the optimal hot working parameters of 20CrMnTiH steel by establishing the hot processing map at different deformation temperature, strain rate and strain conditions by combining the process map with the microstructure during processing.

2. Development of hot processing maps of 20CrMnTiH

2.1 Fundamentals of processing maps

DOI: 10.1080/03019233.2016.1264145

According to the DMM model, the deformed workpiece is considered as a nonlinear energy dissipater and the deformation process was as an energy conservation system. The instantaneously dissipated total power (P) of workpiece during hot working consisted of two complementary parts: one is the power dissipated content (G) by plastic deformation which results in the temperature to be increased, another is the power dissipation co-content (J) caused by metallurgical process which results in the microstructural change. The instantaneously dissipated total power (P) can be described in terms of strain energy at a given temperature in the hot forming regime [15]:

$$P = \bar{\sigma} \cdot \dot{\bar{\varepsilon}} = \int_0^{\dot{\bar{\varepsilon}}} \bar{\sigma} \cdot d\dot{\bar{\varepsilon}} + \int_0^{\bar{\sigma}} \dot{\bar{\varepsilon}} \cdot d\bar{\sigma} = G + J \tag{1}$$

where $\bar{\sigma}$ is the effective stress and $\dot{\bar{\varepsilon}}$ is the effective strain rate.

For a plastically deformed material, the constitutive equation can be defined at a given deformation temperature T, the effective strain rate $\dot{\bar{\varepsilon}}$ and the effective strain $\bar{\varepsilon}$ as follows:

$$\bar{\sigma} = K(T, \bar{\varepsilon}, \dot{\bar{\varepsilon}})\dot{\bar{\varepsilon}}^m \tag{2}$$

where K is strength coefficient, m is the strain rate sensitivity exponent, which defines the relative proportion of total energy between plastic deformation and microstructural change at given temperature and strain， and the value of m can be calculated according to the flow stress obtained from the hot compression experiments. It can be expressed by:

$$\mathrm{m} = \frac{\Delta J}{\Delta G} = \frac{\int_{\bar{\sigma}}^{\bar{\sigma}+\Delta\bar{\sigma}} \dot{\bar{\varepsilon}} d\bar{\sigma}}{\int_{\dot{\bar{\varepsilon}}}^{\dot{\bar{\varepsilon}}+\Delta\dot{\bar{\varepsilon}}} \bar{\sigma}\, d\dot{\bar{\varepsilon}}} = \frac{\dot{\bar{\varepsilon}}\Delta\bar{\sigma}}{\bar{\sigma}\Delta\dot{\bar{\varepsilon}}} = \frac{\dot{\bar{\varepsilon}} d\bar{\sigma}}{\bar{\sigma} d\dot{\bar{\varepsilon}}} = \frac{dln\bar{\sigma}}{dln\dot{\bar{\varepsilon}}} \tag{3}$$

The efficiency of power dissipation η is introduced to represent how efficiently the power dissipates by metallurgical process during plastic deformation. It is defined as a linear dissipater (m=1):

$$\eta = \frac{{}^{\Delta J}/_{\Delta P}}{\left({}^{\Delta J}/_{\Delta P}\right)_{linear}} = \frac{{}^{\Delta J}/_{(\Delta J + \Delta G)}}{\left({}^{\Delta J}/_{\Delta P}\right)_{linear}} = \frac{{}^{m}/_{(m+1)}}{{}^{1}/_{2}} = \frac{2m}{m+1} \tag{4}$$

The efficiency of power dissipation η shows the power dissipation capacity of the deformed workpiece. Its value varies with the deformation temperature and strain rate at a given strain. An equivalent contour map can be plotted to represent the three-dimensional variation of η with temperature, strain rate and strain, which constitutes the power dissipation map used to analyze the microstructure evolution mechanism under different process conditions.

The hot-working conditions with higher efficiency of power dissipation are not necessarily safe regions from

DOI: 10.1080/03019233.2016.1264145

microstructural viewpoint since these could be cracking or damage root causes, thus the evaluation criteria for the flow instability must also be discussed. According to the extremum principles of maximum rate of entropy production, another dimensionless parameter, the instability coefficient ξ, is defined to estimate the regions where flow instability, fracture or defects are most likely to occur. The instability criterion is expressed by:

$$\xi = \frac{\partial \log(\frac{m}{1+m})}{\partial \log \varepsilon} + m < 0 \tag{5}$$

The variation of the instability coefficient ξ with temperature and strain rate at a given strain represents the instability map, which can be applied to predict flow instability or the microstructure defects when $\xi < 0$.

By superimposing the energy dissipation map on the instability map, the hot processing maps can be obtained and the hot-workability will be analyzed according to the processing maps.

2.2 Materials and Experiments

The chemical composition of 20CrMnTiH steel and the hot compression experiment procedures have been described in detail in reference [12] and [13]. The original microstructures of the as-received test steel are consisted of the ferrite and pearlite, as shown in Fig.1. The cylindrical specimens with a diameter of 8mm and a height of 12mm are compressed on the Gleeble-3500 thermal simulator with the temperatures range of 850~1150℃ and the strain rates range of 0.01~1s^{-1} and with a compressive strain 0.916. The flow stress-strain curves can be obtained under different deformation conditions as shown in Fig.2 [12]. All the deformed samples are sectioned along the compression direction in the sample center and the microstructure can be observed by metallographic microscopy.

Based on the flow stress-strain data obtained in Fig.2, the strain rate sensitivity exponent m is calculated under different temperatures, strain rates and strains according Eq. (3), as shown in Table 1.

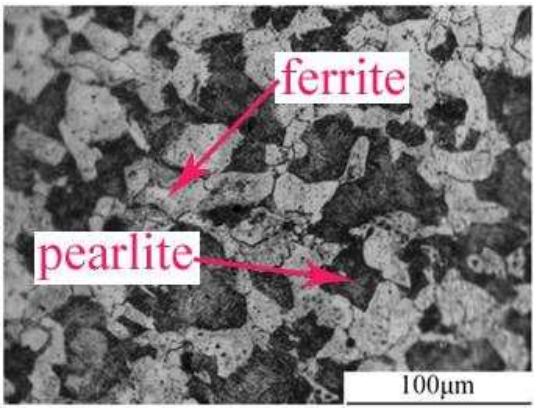

Fig.1. The original optical microstructure of the as-received 20CrMnTiH steel

DOI: 10.1080/03019233.2016.1264145

Table 1 m values of 20CrMnTiH steel under different work conditions

Strain	Strain rate(s^{-1})	Temperature(°C)			
		850	950	1050	1150
0.2	0.01	0.1438	0.1412	0.2667	0.2677
	0.1	0.0997	0.1074	0.2031	0.1952
	1	0.0555	0.0735	0.1396	0.1226
0.4	0.01	0.1498	0.2407	0.2495	0.2369
	0.1	0.1044	0.1684	0.2183	0.1959
	1	0.0590	0.0960	0.1871	0.1548
0.6	0.01	0.1863	0.2097	0.2252	0.2179
	0.1	0.1365	0.1832	0.2075	0.1990
	1	0.0867	0.1567	0.1981	0.1801
0.8	0.01	0.2372	0.2157	0.2306	0.1886
	0.1	0.1717	0.1883	0.2110	0.1861
	1	0.1061	0.1610	0.1914	0.1835
0.916	0.01	0.2184	0.2498	0.2222	0.1952
	0.1	0.1669	0.1855	0.2038	0.1925
	1	0.1154	0.1212	0.1855	0.1898

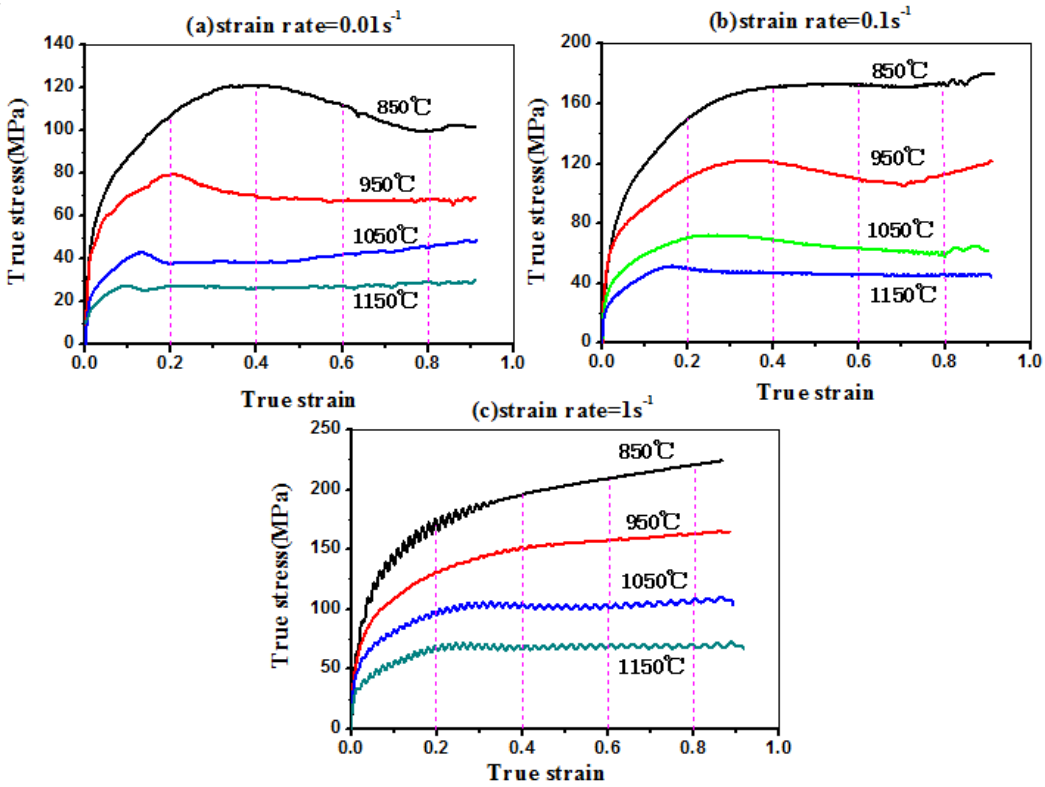

Fig.2. True Stress-Strain curves of 20CrMnTiH steel at different strain rate :(a) $\dot{\varepsilon} = 0.01s^{-1}$; (b) $\dot{\varepsilon} = 0.1s^{-1}$; (c) $\dot{\varepsilon} = 0.1s^{-1}$

DOI: 10.1080/03019233.2016.1264145

2.3 Processing maps of 20CrMnTiH

The m values obtained in Table 1 are used to calculate the efficiency of power dissipation η and the instability coefficient ξ according to Eq. (4) and Eq. (5), thus the power dissipation maps and the instability maps for 20CrMnTiH steel can be obtained under different temperatures, strain rates and strains, respectively, as shown in Fig. 3 and Fig. 4. Fig.3a are the 3D power dissipation maps for 20CrMnTiH steel, which can represent the three dimensional variation of η with temperature, strain rate and strain. Fig.3b-f and Fig.4a-e show the 2D power dissipation maps and the instability maps for 20CrMnTiH steel under different hot work conditions and the contour values indicate the η value and ξ value, respectively. From these results the hot processing maps for 20CrMnTiH steel at the deformation temperature region of 850~1150^{o} C, strain rate 0.01~1s^{-1} and the strain of 0.2~0.916 can be developed by superimposing Fig.3 and Fig.4, as shown in Fig. 5. The contour values represent the η value under different conditions.

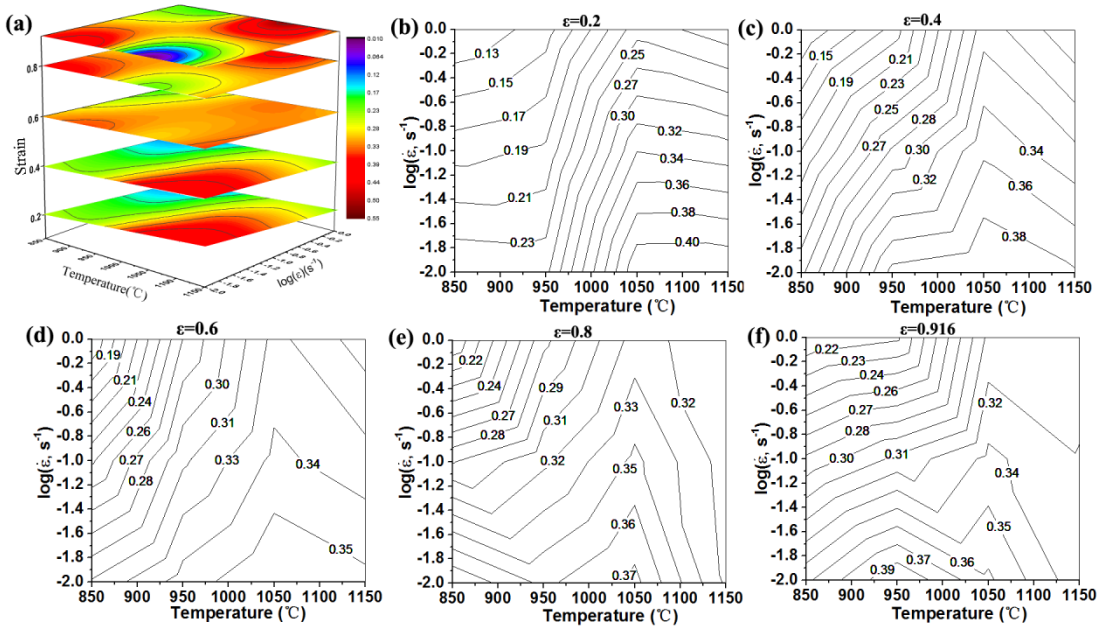

Fig.3 3D and 2D power dissipation maps of 20CrMnTiH steel at different compressive strains

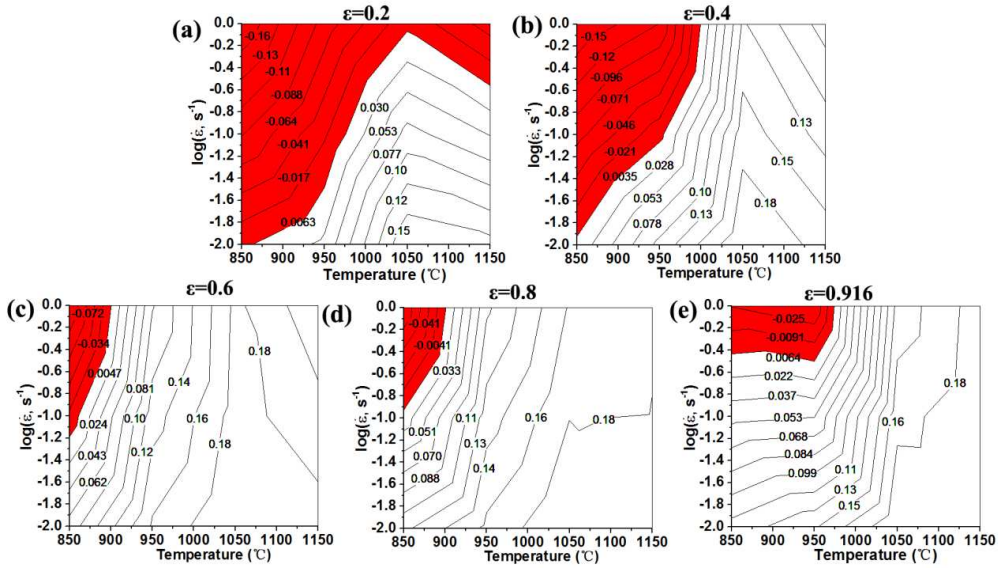

Fig.4 3D and 2D instability maps of 20CrMnTiH steel at different compressive strains

DOI: 10.1080/03019233.2016.1264145

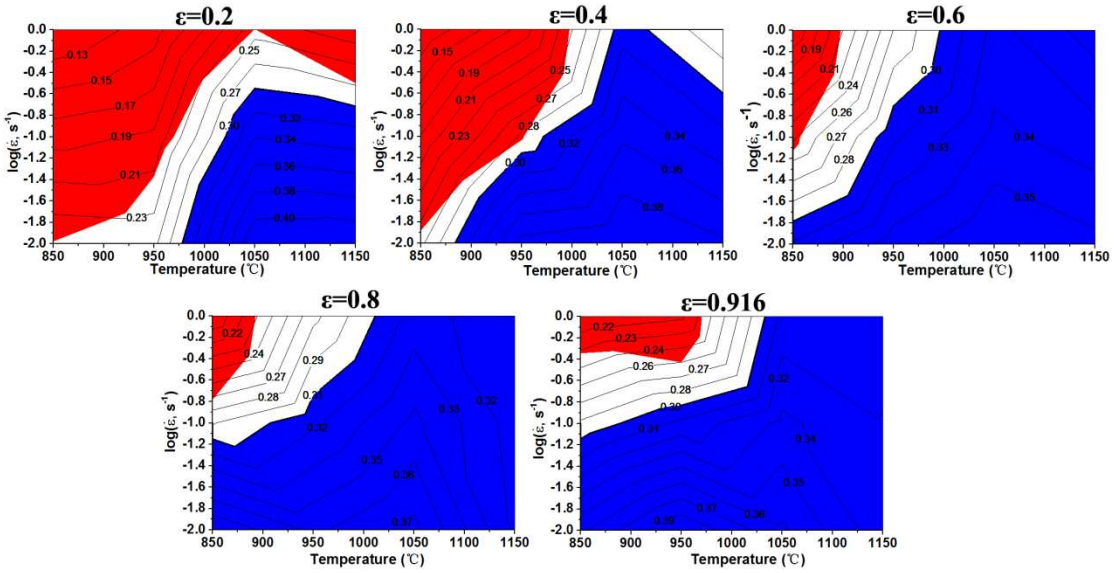

Fig.5 Processing maps of 20CrMnTiH steel at different compressive strains

3. Results and discussions

3.1 Safe region and Instability region

Generally, the efficiency of power dissipation η represents the rate of microstructural evolution occurred due to hot deformation. That is to say, the regions with a higher η value in the power dissipation map means that the material is of the better hot workability and easier to achieve microstructure evolution. According to Fig.3, the efficiency of power dissipation η varies with the strain. The peak η value increases firstly then decreases with increasing strain and occur at high temperature and low strain rate when strain value is at 02~0.6 and also exists at moderate-temperature and lower strain rate when strain is at 0.8~0.916. The peak values of η are 0.4, 0.38, 0.35, 0.37 and 0.39 at the strain values of 0.2, 0.4, 0.6, 0.8 and 0.916, respectively. In the light of the previous research [12-14] and Fig.2, the stress-strain curves for 20CrMnTiH steel exhibit the dynamic recovery (DRV) and dynamic recrystallization (DRX) softening mechanism. The flow stress, which increasing rapidly first then flattening out gradually with increasing strain, indicates that the DRV behavior takes place at low temperature and high strain rate. The flow stress curves with peak at the high temperature and low strain rate show that the DRX is the dominant deformation mechanism and the deformed material is of larger DRX degree at higher temperature. The DRX behavior is accompanied by the higher power dissipation to provide energy to the grain nucleation and growth.

Regions with high power dissipation efficiency is not necessarily safe regions for defect free deformation due to the complexity of the microstructure evolution [6], the instability map is used to estimate the instability regions for the deformed material. On the basis of the instability criterion, the instability regions with negative ξ values for 20CrMnTiH steel are marked in red color in Fig.4 and they occur at the higher strain rate and lower temperature. From Fig.4 there are two instability regions at the strain value of 0.2. One region occurs at the temperature range of 850~1050ºC and the strain rate range of 0.01~1s^{-1}, another one is at the temperature range of 1050~1150ºC and the strain rate range of 0.324~1s^{-1}. The instability region exists at the temperature range of 850~997ºC and the strain rate range of 0.013~1s^{-1}, and at the temperature range of 850~898ºC and the strain rate range of 0.077~1s^{-1} and at the temperature range of 850~891ºC and the strain rate range of 0.169~1s^{-1}, and at the temperature range of 850~950ºC and the strain rate range of 0.38~1s^{-1} , and at the temperature range of 850~971ºC and the strain rate range of 0.371~1s^{-1} at the strain of 0.4, 0.6, 0.8, 0.916, respectively. These instability regions are considered as unsafe deformation zones, which resulted from deformation defects, such as flow localization, adiabatic shear band

DOI: 10.1080/03019233.2016.1264145

and cracking [8,16] and should be avoided during hot forming of 20CrMnTiH steel.

Generally, the processing maps are used to identify different deformation domains with various microstructural mechanisms, such as DRV, DRX and superplastic deformation which considered as safe mechanisms in terms of the safe regions, without the void formation, wedge cracking, intercrystalline cracking, flow localization and adiabatic shear band which depict damage mechanisms named instability region [6,9].

As seen from Fig.5, the processing map of 20CrMnTiH steel is of different characteristics with the increasing strain from 0.2 to 0.916. The instability regions occur at both low temperature with all strain rates and at high temperature with high strain rate at the strain of 0.2. And the area of instability gradually decreases with the increasing strain and only emerges at lower temperature and higher strain rate with the strain value of over 0.2.

DRX imparts excellent hot workability to the material and is desirable for hot forming of many metal materials [6]. Therefore, to bring about the grain refinement and to improve the mechanical properties of the deformed parts, it is desirable that the DRX behavior occurs during hot forming products of 20CrMnTiH steel. Referred to the DRX kinetics, the nucleation of the DRX grain initiates at the critical strain ε_c, $\varepsilon_c = 0.8\varepsilon_p$, where ε_p is the peak strain and can be decided according to strain-stress curve of Fig.2. Thus ε_c can be calculated by Fig.2 and used to evaluate whether the DRX behavior occurs or not, as shown in Table 2. As can be seen from Table 2, the critical strain ε_c is affected obviously by temperature and the strain rate and the DRX behavior does not occur at low temperatures and high strains. Thus the η values caused the DRX phenomenon under different deformation conditions are calculated according to Table 1, Table 2 and Eq. (4), as shown in Table **3**. As can be seen from Table 3, the η values corresponding to the occurrence of DRX are approximately over 0.22 and the η values are approximately in the range of 0.3~0.40 when the strain is over 0.4, which is in agreement with the results of the previous reports [11,15]. Therefore, the safe and instability regions with higher η values ($\geqslant$0.3) under different strains for 20CrMnTiH steel can be determined. In fig.5, the regions in red show the instability domains resulted from deformation defects, such as flow localization, adiabatic shear band and cracking, and the regions in blue represent the safe domains ($\eta \geqslant 0.3$) with good workability corresponding to the DRX mechanism.

Table 2 The critical strain ε_c under different conditions

ε_c	0.01s^{-1}	0.1 s^{-1}	1 s^{-1}
850℃	0.302	--	--
950℃	0.163	0.276	--
1050℃	0.106	0.198	0.246
1150℃	0.077	0.130	0.195

Table 3 The η values corresponding DRX under different conditions

Strain	Strain Rate(s^{-1})	Temperature(°C)			
		850	950	1050	1150
0.2	0.01	--	0.25	0.42	0.42
	0.1	--	--	0.34	0.33
	1	--	--	--	0.22
0.4	0.01	0.26	0.39	0.40	0.38
	0.1	--	0.29	0.36	0.32
	1	--	--	0.32	0.27
0.6	0.01	0.31	0.36	0.37	0.36
	0.1	--	0.32	0.34	0.31
	1	--	--	0.33	0.31
0.8	0.01	0.38	0.36	0.37	0.32
	0.1	--	0.32	0.35	0.31
	1	--	--	0.32	0.31
0.916	0.01	0.36	0.40	0.36	0.33
	0.1	--	0.31	0.34	0.32
	1	--	--	0.31	0.32

DOI: 10.1080/03019233.2016.1264145

3.2 Validation of processing maps

The typical optical microstructure corresponding to the red and blue region in Fig.6 and Fig.7 are observed to validate the processing window decided by the processing map. Fig.6 shows the SEM micrographs at different temperatures and strain rates at the strain 0.916. The localized flow of the deformed specimen at 850ºC/1s^{-1} and 950ºC/1$s^{-1}$is observed as shown in Fig. 6(a) and (b). The microstructure distribution is very uniform at 1050ºC/1s^{-1} and 1150/0.1 s^{-1} as shown in Fig. 6(c) and (d). Generally, DRX is very limited at low temperature and adiabatic heating is difficult to be conducted at high strain rate due to a shorter deformation time, which can result in flow localization [8, 11].

Fig.7 shows the microstructure characteristics of the deformed samples at different working conditions at the strain 0.916. Fig. 7(a) and (b) show the unstable region microstructure obtained at 850 ºC/1s^{-1} and 950ºC/1s^{-1}, respectively. It can be seen that the microstructure in unstable region is elongated and the necklace structure has occurred, caused by the local plastic flow and should be avoided due to weakening the mechanical properties of the steel during hot processing. Fig. 7(c)-(i) represent the microstructure at the safe region with higher η value, respectively. It can be seen that the microstructures in safe region are of equiaxial DRX grains, which shows the full DRX behavior occurred under these processing conditions. These results agree with the ones obtained from the processing map.

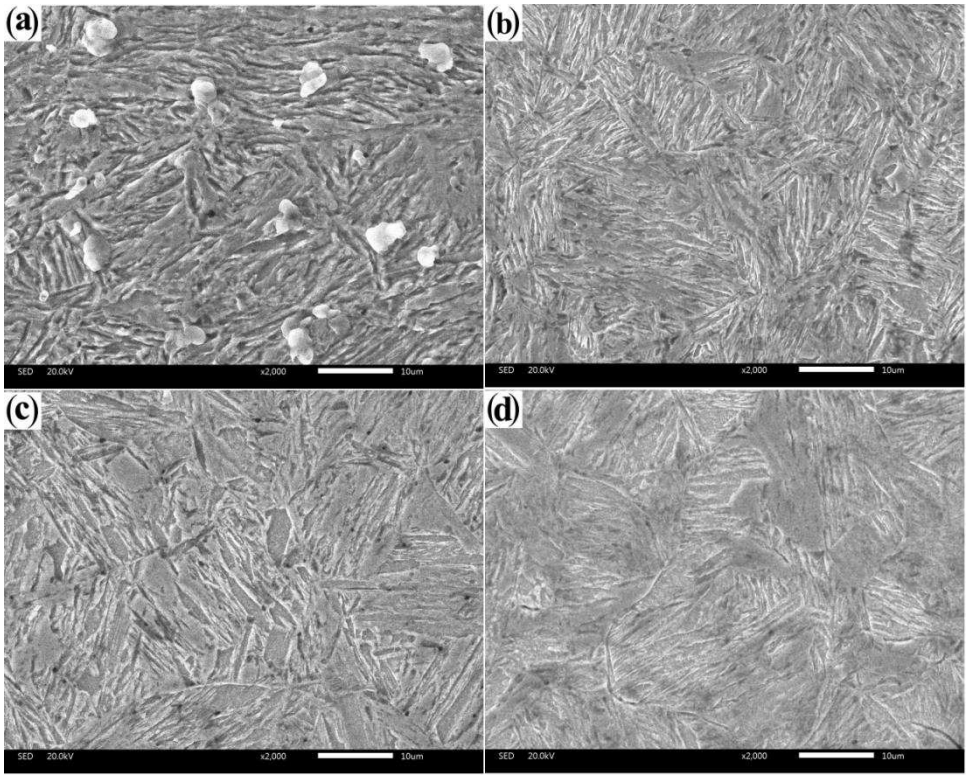

Fig.6 SEM micrographs of 20CrMnTiH steel at a strain of 0.1916: (a) 850ºC,1s^{-1};(b) 950ºC,1s^{-1}; (c) 1050ºC,0.01s^{-1}; (d) 1050ºC,1s^{-1}

DOI: 10.1080/03019233.2016.1264145

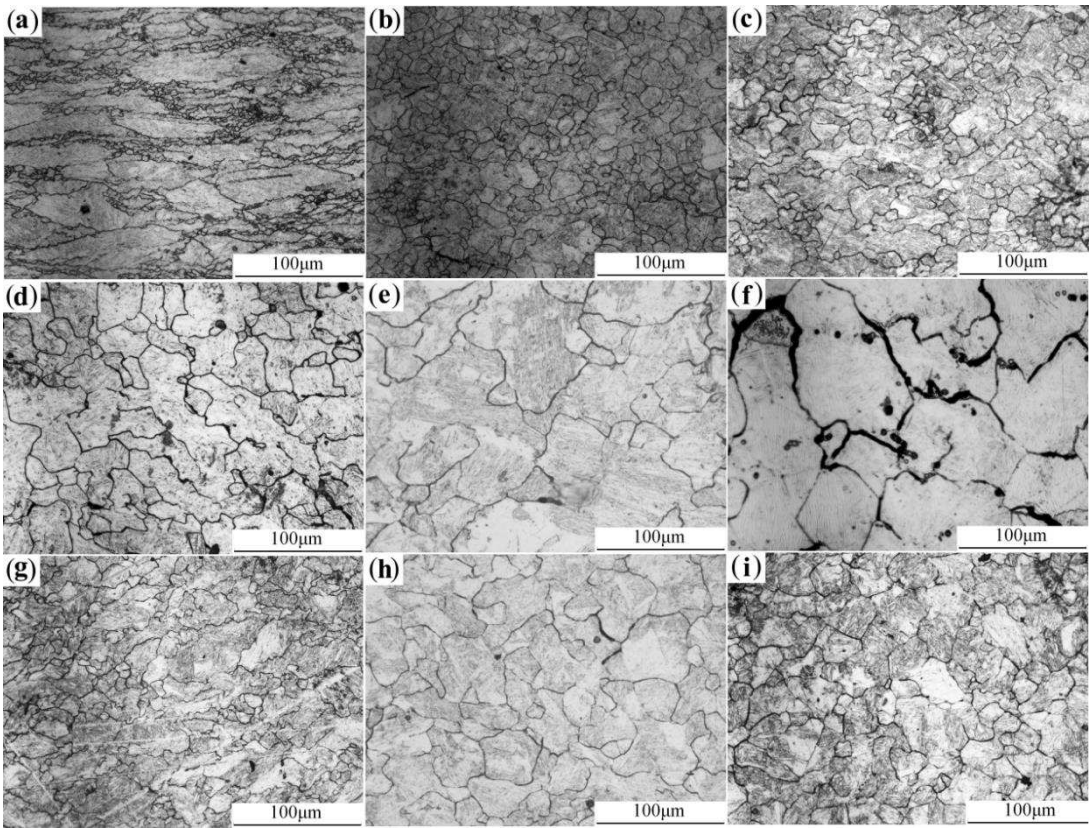

Fig.7 Optical micrographs of 20CrMnTiH steel at a strain of 0.1916: (a) 850ºC/1s^{-1}; (b) 950ºC/1s^{-1}; (c) 850ºC/0.01s^{-1}; (d) 950ºC/0.01s^{-1}; (e) 1050ºC/0.01s^{-1}; (f) 1150ºC/0.01s^{-1}; (g) 950ºC/0.1s^{-1}; (h) 1050ºC/0.1s^{-1}; (i) 1050ºC/1s^{-1}

3.3 Optimization of processing window

Combing the analysis of processing map with the microstructure observation, the optimum processing window for 20CrMnTiH steel can be obtained.

In Fig. 7(c)-(i), it can be seen that the DRX grain structures are obviously affected by deformation temperature and strain rate. The grain sizes increase with increasing temperature at the same strain rate as shown in Fig. 7(c)-(f) and (g)-(h), respectively. However, the DRX degree is greater and the distribution of the microstructure is more uniform at high temperatures. This because that the nucleation and growth of DRX grain are a thermally-activation processing, which can be accelerated with the increasing temperature [17]. While the grain sizes decrease with the increase of strain rate at the same temperature as shown in Fig. 7(d)-(g) and (e), (h),(i), respectively. This attributes to the fact that high strain rate provides less time for the movements of grain boundaries and dislocation, which postpones the nucleation and growth of DRX grains. The average DRX grain sizes measured in Fig.7 (c)-(i) according linear intercept method are 14.8μm, 24.34μm, 47.03μm, 68.05μm, 17.13μm, 29.54μm, and 22μm at 850ºC/0.01s^{-1}, 950ºC/0.01s^{-1}, 1050ºC/0.01s^{-1}, 1150ºC/0.01s^{-1}, 950ºC/0.1s^{-1}, 1050ºC/0.1s^{-1} and 1050ºC/1s^{-1}, respectively. Generally, the grain sizes of the product should be in the range of 22-30μm to meet the mechanical properties required in industry applications. Though the η value is higher at 1050ºC/0.01s^{-1} and 1150ºC/0.01s^{-1}, the DRX grain sizes are relatively large and these processing parameters are not the optimum. Thus, the optimum processing window for 20CrMnTiH steel can be obtained combining the processing map and the DRX behavior analysis in order to optimize the hot workability and control the microstructure. That is to say, in forming 20CrMnTiH steel the processing parameters should be designed in these regions, where the material is not only of having higher η value but also with larger DRX degree to achieve smaller grain sizes. Therefore, it can be concluded

DOI: 10.1080/03019233.2016.1264145

that the domains at a low temperature and strain rate or a high temperature and strain rate are beneficial to hot-working, grain refinement and uniform microstructure with full DRX. Finally, the optimum processing parameters of 20CrMnTiH steel during hot deformation at a strain value of 0.916 are 1036-1070℃/0.1-1s^{-1} and 918-985℃/0.01-0.014s^{-1}.

Conclusions

The hot processing maps of 20CrMnTiH steel are developed using the principles of dynamic materials models based on the stress strain data obtained using hot compression tests. The safe and instability deformation regions are identified and the hot workability is evaluated according to the processing maps. The optimum processing parameters are obtained by combining the processing map with DRX behavior. The main conclusions can be drawn from this study as follows:

1) The efficiency of power dissipation η varies with the strain; the peak value of η increases firstly then decreases with increasing strain and occurs at high temperature and low strain rate when strain is 02~0.6 and also occurs at high temperature high strain rate when strain is 0.8~0.916. At the safe regions, when the η values are over 0.3~0.5, the DRX mechanism is prominent and the steel is of good hot workability.

2) The instability regions occur at both low temperature with all strain rate and high temperature with high strain rate at the strain of 0.2. And the area of instability gradually decreases with the increasing strain and only exists at lower temperature and higher strain rate when the strain is greater than 0.2. The instability region exhibits flow localization confirmed by the microstructure observation.

3) The optimum processing parameters during hot working 20CrMnTiH steel are 1036-1070℃/0.1-1s^{-1} and 918-985℃/0.01-0.014s^{-1}.

Acknowledgements

Dr. Wei Feng would like to acknowledge the support of the State Scholarship Fund of China Scholarship Council for supporting her study as a visiting scholar in The University of Sheffield, UK. The authors would also like to thank funding support to this research from the Natural Science Foundation of China (No. 51475344) and the Natural Science Foundation of Hubei Province (2014CFB855), Innovative Research Team Development Program of Ministry of Education of China (IRT13087).

References

[1] S.K. Rajput, M. Dikovits, G.P.Chaudhari,C.Poletti, F.Warchomicka,V.Pancholi,S.K.Nath. Physical simulation of hot deformation and microstructural evolution of AISI 1016 steel using processing maps. Materials Science & Engineering A, 2013; 587: 291-300.

[2] Y. V. R. K. Prasad, H. L. Gegel, S. M. Doraivelu, J. C. Malas, J. T. Morgan, K. A. Lark and D. R. Barker. Modelling of dynamic behavior in hot deformation: forging of Ti-6242. Metall Trans A, 1984; 15:1883-1892.

[3] Y. V. R. K. Prasad. Processing Maps:A Status Report. Journal of Materials Engineering and Performance,2013,22(10):2867-2874.

[4] Prasad, K, P. Rao. Processing maps and rate controlling mechanisms of hot deformation of electrolytic tough pitch copper in the temperature range 300-950℃. Materials Science and Engineering A, 2005; 391:141-150.

[5] Y. V. R. K. Prasad, K. P. Rao. Processing maps for hot deformation of rolled AZ31 magnesium alloy plate: Anisotropy of hot workability. Materials Science and Engineering A, 2008; 487: 316-327.

DOI: 10.1080/03019233.2016.1264145

[6] R.S.Septimio, S.T.Button,C.J.V.Tyne. Processing maps for the ananlysis of hot workability of microalloyed steels 38MnSiVS5 and 0.39C1.47Mn. J Mater Sci, 2016,51:2512-2528.

[7] H. Rastegari, A. Kermanpur, A. Najafizadeh, D. Porter, M. Somani. Warm deformation processing maps for the plain eutectoid steels. Journal of Alloys and Compounds, 2015,626:136-144.

[8] Zhinan Yang, Fucheng Zhang, Chunlei Zhang, Ming Zhang, Bo Lv, Lin Qu. Study on hot deformation behaviour and processing maps of low carbon bainitic steel. Materials and Design, 2015,66:258-266.

[9] Yang Cheng, H uayun Du, Yinghui Wei, Lifeng Hou, Baosheng Liu. Metadynamic recrystallization behavior and workability characteristics of HR3C austenitic heat-resistant stainless steel with processing map. Journal of Materials Processing Technology, 2016, 235:134-142.

[10] Li Miaoquan, Zhang Xiaoyuan. Optimization of TC11 alloy forging parameters using processing maps. Rare Metals, 2011,30(3):222-226.

[11] G. Z. Quan, L. Zhao, T. Chen, Y. Wang, Y. P. Mao, W. Q. Lv and J. Zhou. Identification for the optimal working parameter of as-extruded 42CrMo high- strength steel from a large range of strain rate and temperature. Materials Science and Engineering A, 2012; 538: 364-373.

[12] W. Feng, Y. H. Fu. High temperature deformation behavior and constitutive modeling for 20CrMnTiH steel, Materials and Design. 2014; 57: 465-471.

[13] S. T. Wu, W. Feng and X. Hu. Constitutive modeling of flow bahaviour of 20CrMnTiH steel, Ironmaking & Steelmaking. 2015; 42(7): 481-488.

[14] W. Feng, F. J. Xu. Microstructure evolution and dynamic recrystallization model of 20CrMnTiH steel during compression, Journal of Plasticity Engineering. 2014; 21(3): 78-84.(in Chinese)

[15] H. Ziegler. Some extremum principles in irreversible thermodynamics with applications to continuum mechanics. Progress in Solid Mechanics,1965,4:91-193

[16] E. X. Pu, W. J. Zheng, J. Z. Xiang, Z. G. Song, J. Li. Hot deformation characteristic and processing map of superaustenitic stainless steel S32654, Materials Science & Engineering A. 2014,598: 174-182.

[17] Y.C.Lin, D.G.He,M.S.Chen,X.M.Chen,C.Y.Zhao,X.Mao,Z.L. Long. EBSD analysis of evolution of dynamic recrystallization grains and δ phase in a nickel-based superalloy during hot compressive deformation. Materials and Design,2016,97:13-24.